A complex-valued fMRI data model for both the magnitude and phase

Daniel B. Rowe

Division of Biostatistics
Medical College of Wisconsin

Technical Report 48

November 2004

Division of Biostatistics
Medical College of Wisconsin
8701 Watertown Plank Road
Milwaukee, WI 53226
Phone:(414) 456-8280

A complex-valued fMRI data model for both the magnitude and phase

Daniel B. Rowe*
Department of Biophysics
Medical College of Wisconsin
Milwaukee, WI USA

Abstract

In MRI and fMRI, images or voxel measurements are complex valued or bivariate at each time point. Recently Rowe and Logan (2004) introduced an fMRI magnitude activation model that utilized both the real and imaginary data in each voxel. This model, following traditional beliefs, specified that the phase time courses were fixed unknown quantities which may be estimated voxel-by-voxel. Subsequently, Rowe and Logan (2005) generalized the model to have no restrictions on the phase time courses. They showed that this unrestricted phase model was mathematically equivalent to the usual magnitude-only data model including regression coefficients and voxel activation statistic but philosophically different due to its derivation from complex data. Recent findings by Hoogenrad (1998) and Menon (2002) indicate that the voxel phase time course may exhibit task related changes. In this paper, a general complex fMRI activation model is introduced that describes both the magnitude and phase in complex data which can be used to specifically characterize task related changes in both. Hypotheses regarding task related magnitude and/or phase changes are evaluated using derived activation statistics. It was found that the the Rowe-Logan complex constant

*Corresponding Author: Daniel B. Rowe, Department of Biophysics, Medical College of Wisconsin, 8701 Watertown Plank Road, Milwaukee, WI 53226, dbrowe@mcw.edu.

phase model strongly biases against voxels with task related phase changes and that the the current very general complex linear phase model can be cast to address several different hypotheses sensitive to different magnitude/phase changes.

1 Introduction

It is well known that in magnetic resonance imaging (MRI) and functional magnetic resonance imaging (fMRI), images or voxel measurements are complex valued or bivariate due to phase imperfections and thus in fMRI, voxel time course measurements appear in both the real and imaginary channels [2, 6, 10]. An example of a voxels' complex valued time course with assumed magnitude task related changes and a constant phase is presented in Fig. 1 where the length of the vector from the origin to the point in real-imaginary space is the magnitude and the angle the vector makes with the real axis is the phase. In fMRI, the real and imaginary components are the quantities that are measured with observation error. In for example a block design finger tapping experiment, the vector described by the arrow in Fig. 1 appears to "jitter" around in a lower vector length state during the control task then the length of this vector increases and the vector appears to "jitter" around in a higher vector length state. Any apparent "jitter" in the phase would be purely from measurement error in the real and imaginary components of the vector. In fMRI, complex valued voxel time courses are generally converted to magnitude and phase time courses then task related magnitude-only data activation determined with the phase voxel time course discarded [1, 3]. The original complex data are unrecoverable after discarding the phase and the magnitude-only operation is nonunique. Other attempts have been made to avoid complex voxel time courses such as phasing them into the real channel [2].

Rowe and Logan (2004) introduced a general complex fMRI magnitude activation model in which multiple regressors were allowed using the standard general linear statistical model, hypothesis tests were formulated in terms of contrasts, and the phase was directly modeled as a fixed unknown quantity which may be estimated voxel by voxel [16]. Further, a large sample chi-square distributed statistic was presented. In Rowe and Logan (2005) the complex model was generalized to have an unrestricted phase time course [17]. They showed that this model

Figure 1: Complex valued voxel time course.

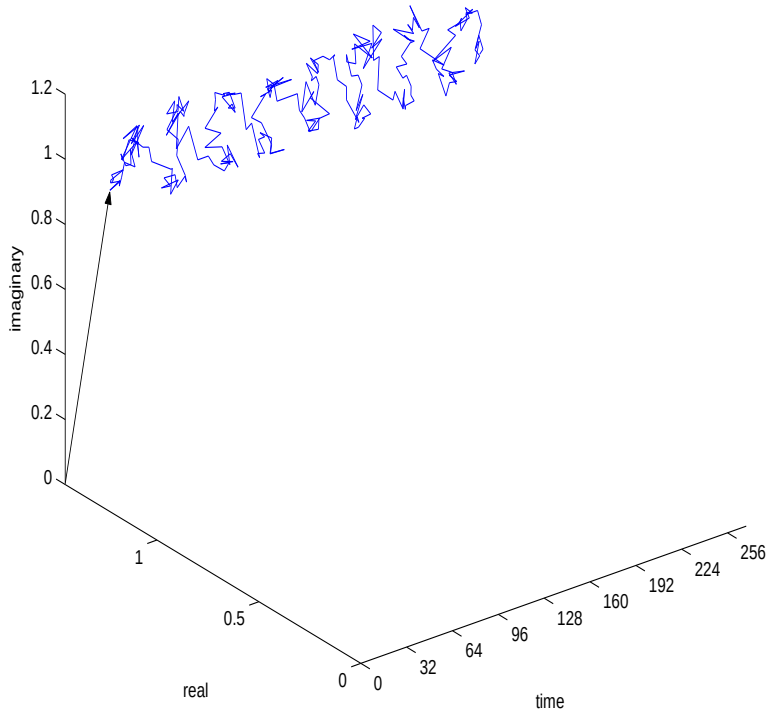

was mathematically equivalent to the usual magnitude-only data model in terms of regression coefficients and voxel activation statistic but philosophically different due to its derivation from complex data. The magnitude-only or equivalently complex unrestricted phase data models only utilize information in the magnitude through the exact Ricean distribution or through the large SNR normal distribution approximation [5, 13].

However, recently Hoogenrad (1998) and Menon (2002) presented evidence to suggest that the voxel phase angle time courses may not be exactly constant over time but may also exhibit task related phase changes in voxels with "large" vessels [7, 11]. In this paper, a general complex fMRI activation model is introduced that describes both the magnitude and phase which can be used to specifically model and test for task related changes in the magnitude, the phase, or both the magnitude and phase. Thus in principle activation can be determined from voxels with "small" vessels such as those in the capillary bed of parenchymal tissue having solely magnitude changes and not voxels with "large" vessels having task related changes in both the magnitude and phase. This implies that the phase may contain information about the brain that is not present in the magnitude of the response.

The situation of the vector valued voxel observation residing in the two magnitude length states is depicted in Fig. 2a while the situation of the two vector states that involve a lengthening and rotation is depicted in Fig. 2b.

The activation model from magnitude-only data is sensitive to voxels that have task related changes in the magnitude regardless of whether there are changes of any kind in the phase, while magnitude activation from complex data specifically describes and dictates whether or not we wish to include voxels that have task related phase changes. Recent work by Hoogenrad (1998) and Menon (2002) indicates that there can be task related phase changes, especially for voxels with "larger" venous fractions. Menon sought to account for changes in the observed magnitude that could be accounted for by changes in the phase by including voxel phase values as a random independent regressor variable in a least squares model [7, 11].

Figure 2: Task related magnitude/phase changes.

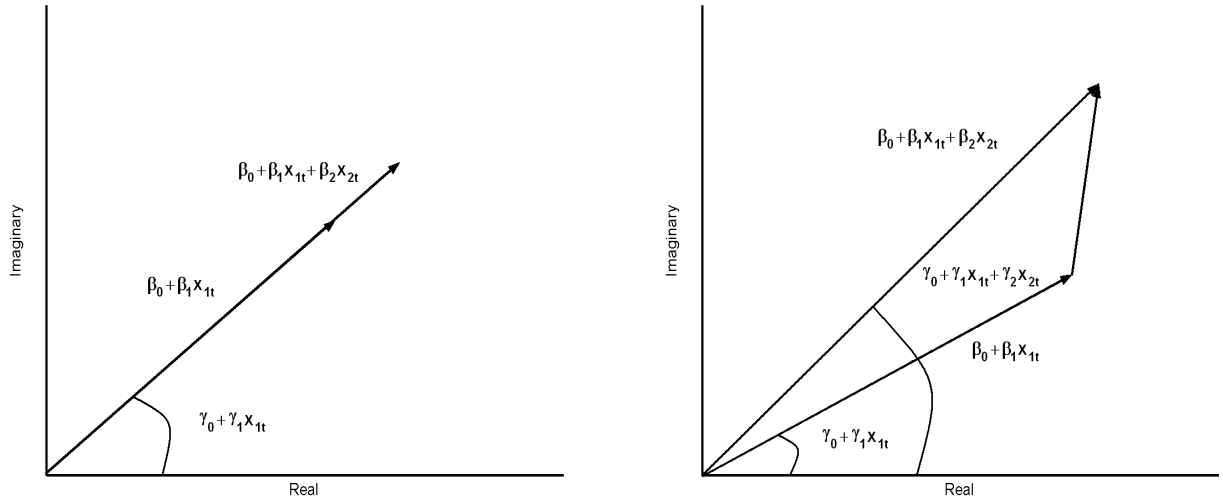

(a) Magnitude-alone change

(b) Magnitude and phase change

In fMRI we seek voxels with small vessels in parenchymal tissue having random orientations whose phase contributions are small in aggregate. Thus, in principle, the phase angle contains information about the vasculature in the vicinity of the voxel. It is this information that is sought to model and utilize. A generalization of the Rowe-Logan (2004,2005) complex activation models is developed where the phase angle can be described with a linear

model where task related changes in the phase can be quantified. With this model, several pairs of hypotheses can be tested including determining voxels that exhibit task related magnitude-alone changes, phase-alone changes, along with task related magnitude and/or phase changes. Task related magnitude and/or phase activation maps can be generated from complex valued voxel time courses and an appropriate threshold determined [9].

Results of the proposed complex linear phase model with five different hypothesis pairs are compared to a complex unrestricted phase or strict magnitude-only data model, a phase-only data model, and the Rowe-Logan complex constant phase data model in terms of thresholded activation maps for a real dataset then activation power for simulated data. The simulations are performed with several magnitude contrast-to-noise ratios (CNRs) and task related phase changes (TRPC) for two different signal-to-noise ratios (SNRs).

2 Model

As previously noted, in MRI/fMRI due to random noise, phase imperfections, and possible biophysical processes that produce phase signal variation, we obtain a complex valued measured object that consists of a true complex valued object plus complex valued noise.

Neglecting the voxel location and focusing on an individual voxel, the complex valued image y_t measured over time t can be described with a nonlinear multiple regression model that includes both a temporally varying magnitude ρ_t and phase θ_t given by

$$\begin{aligned} y_t &= [\rho_t \cos\theta_t + \eta_{Rt}] + i[\rho_t \sin\theta_t + \eta_{It}] \\ \rho_t &= x_t'\beta = \beta_0 + \beta_1 x_{1t} + \cdots + \beta_{q_1} x_{q_1 t} \\ \theta_t &= u_t'\gamma = \gamma_0 + \gamma_1 u_{1t} + \cdots + \gamma_{q_2} u_{q_2 t}, \qquad t = 1, \ldots, n \end{aligned} \tag{2.1}$$

where $(\eta_{Rt}, \eta_{It})' \sim \mathcal{N}(0, \Sigma)$, x_t' is the t^{th} row of a design matrix X for the magnitude, u_t' is the t^{th} row of a design matrix U for the phase, and $\Sigma = \sigma^2 I_2$ while β and γ are magnitude and phase regression coefficient vectors respectively. Note that a separate design matrix for the phase has been incorporated but they can be the same. If $\gamma_j = 0$ for $j = 1, \ldots, q_2$ then this becomes the Rowe-Logan constant phase model. The complex valued observation y_t can

be represented at time point t as a 2×1 vector instead of as a complex number

$$\begin{pmatrix} y_{Rt} \\ y_{It} \end{pmatrix} = \begin{pmatrix} \rho_t \cos\theta_t \\ \rho_t \sin\theta_t \end{pmatrix} + \begin{pmatrix} \eta_{Rt} \\ \eta_{It} \end{pmatrix}, \qquad t = 1, \ldots, n \ .$$

The distributional specification is on the real and imaginary parts of the voxel signal and not on the magnitude or length of a vector. The phase signal in Eq. 2.1 is a temporally varying quantity, which is described with a general linear model and estimated voxel by voxel.

The Rowe-Logan complex fMRI activation models can be written more generally as

$$\underset{2n \times 1}{y} = \underset{2n \times 2n}{\begin{pmatrix} A_1 & 0 \\ 0 & A_2 \end{pmatrix}} \underset{2n \times 2(q_1+1)}{\begin{pmatrix} X & 0 \\ 0 & X \end{pmatrix}} \underset{2(q_1+1) \times 1}{\begin{pmatrix} \beta \\ \beta \end{pmatrix}} + \underset{2n \times 1}{\eta} \tag{2.2}$$

where the observed vector of data $y = (y_R', y_I')'$ is the vector of observed real values stacked on the vector of observed imaginary values and the vector of errors $\eta = (\eta_R', \eta_I')' \sim \mathcal{N}(0, \Sigma \otimes \Phi)$ is similarly defined. Here we specify that $\Sigma = \sigma^2 I_2$ and $\Phi = I_n$. Further, A_1 and A_2 are square diagonal matrices with t^{th} diagonal element $\cos\theta_t$ and $\sin\theta_t$, respectively.

3 Activation

With this model, there are four hypotheses that can readily be seen as presented in Table 1. The parameters are estimated under each of the hypotheses so that pairs of hypotheses can be used in a generalized likelihood ratio test. The existing hypotheses of magnitude-only data activation and magnitude activation from complex data with constant phase are supported within this framework. This framework allows for additional hypotheses regarding task related activation in the magnitude and/or phase in complex data. As previously noted, voxels with task related magnitude and phase changes or activation are potentially ones that contain large vessels and not those that we seek in parenchymal tissue with small vessels.

Denote the maximum likelihood estimators under the alternative hypothesis using hats and those under the null hypothesis using tildes. Then the generalized likelihood ratio statistic for this task related magnitude and/or phase complex fMRI activation model is

$$-2\log\lambda = 2n\log\left(\frac{\tilde{\sigma}^2}{\hat{\sigma}^2}\right) \ . \tag{3.1}$$

$$
\begin{aligned}
H_a &: C\beta \neq 0, \quad D\gamma \neq 0 \\
H_b &: C\beta = 0, \quad D\gamma \neq 0 \\
H_c &: C\beta \neq 0, \quad D\gamma = 0 \\
H_d &: C\beta = 0, \quad D\gamma = 0
\end{aligned}
$$

Table 1: Some possible hypotheses for testing.

This statistic has an asymptotic χ^2_r distribution where r is the difference in the number of constraints between the alternative and null hypotheses. Denoting r_1 and r_2 as the full row ranks of C and D respectively, the degrees of freedom is either r_1, r_2, or $r_1 + r_2$. For example, consider a model with a magnitude design matrix with three columns, the first being ones, the second being counting numbers, and the last being a stimulus or task related reference function along with a phase design matrix that is identical to the magnitude one. The magnitude and phase regression coefficients β_0 and γ_0 represent intercepts; β_1 and γ_1 representing a linear drift over time; while β_2 and γ_2 represent task related effects. Then for example, in hypothesis H_d, the linear coefficient constraints of $H_d : \beta_2 = 0,\ \gamma_2 = 0$ can be described by $C = (0, 0, 1)$ and $D = (0, 0, 1)$ so that the null hypothesis is $H_d : \beta_2 = 0, \gamma_2 = 0$. It should be noted that the Rowe-Logan (2004) complex constant phase model is equivalent to the hypothesis test of H_d vs H_c with $D = (0, I_{q_2})$ or H_b vs H_a with $U = (1, ..., 1)'$ and $D = 1$ while the complex unrestricted phase model is equivalent to a hypothesis test of H_b vs H_a with $U = I_n$ and $D = I_n$.

4 Real fMRI Data

A bilateral sequential finger tapping experiment was performed in a block design with 16s off followed by eight epochs of 16s on and 16s off. Scanning was performed using a 1.5T GE Signa in which 5 axial slices of size 96×96 were acquired with a full k-space single shot gradient echo pulse sequence having a $FA = 90^\circ$ and a $TE = 47$ms. In image reconstruction, the acquired data was zero filled to 128×128. After Fourier image reconstruction, each voxel has dimensions in mm of $1.5625 \times 1.5625 \times 5$. Observations were taken every TR= 1000ms

Figure 3: Thresholded 5% FDR χ^2-statistic activation and overlap maps.

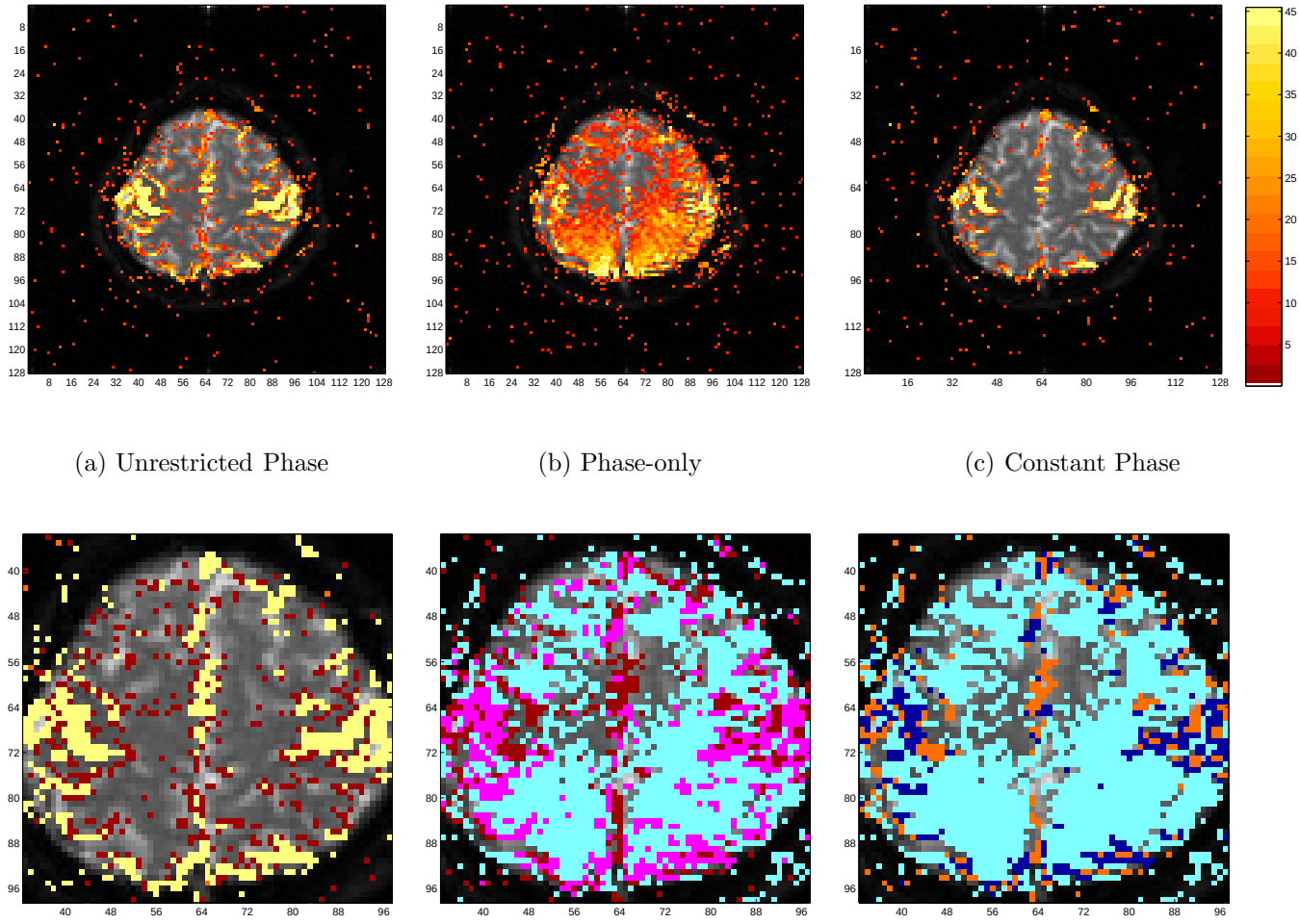

(a) Unrestricted Phase (b) Phase-only (c) Constant Phase

(d) Overlap map UP & CP (e) Overlap map UP & PO (f) Overlap map CP & PO

so that there are 272 in each voxel. Data from a single axial slice through the sensorimotor cortex was selected for analysis. Pre-processing included the removal of the first three points to omit magnetic field equalization effects followed by the use of an ideal 0/1 frequency filter [4, 12] to remove respiration and low frequency physiological noise. Where necessary, the phase time courses were unwrapped for jumps greater than π between successive observations.

In Fig. 3a-c are 5% FDR thresholded χ^2-statistic maps with real fMRI data for (a) the complex unrestricted phase (UP) or usual magnitude-only data model; (b) and a phase-only (PO) data model (activation from phase-only data assuming normality); (c) the Rowe-Logan complex constant phase (CP) activation model; along with overlap maps in (d)-(f) zoomed

Figure 4: Thresholded 5% FWE χ^2-statistic activation and overlap maps.

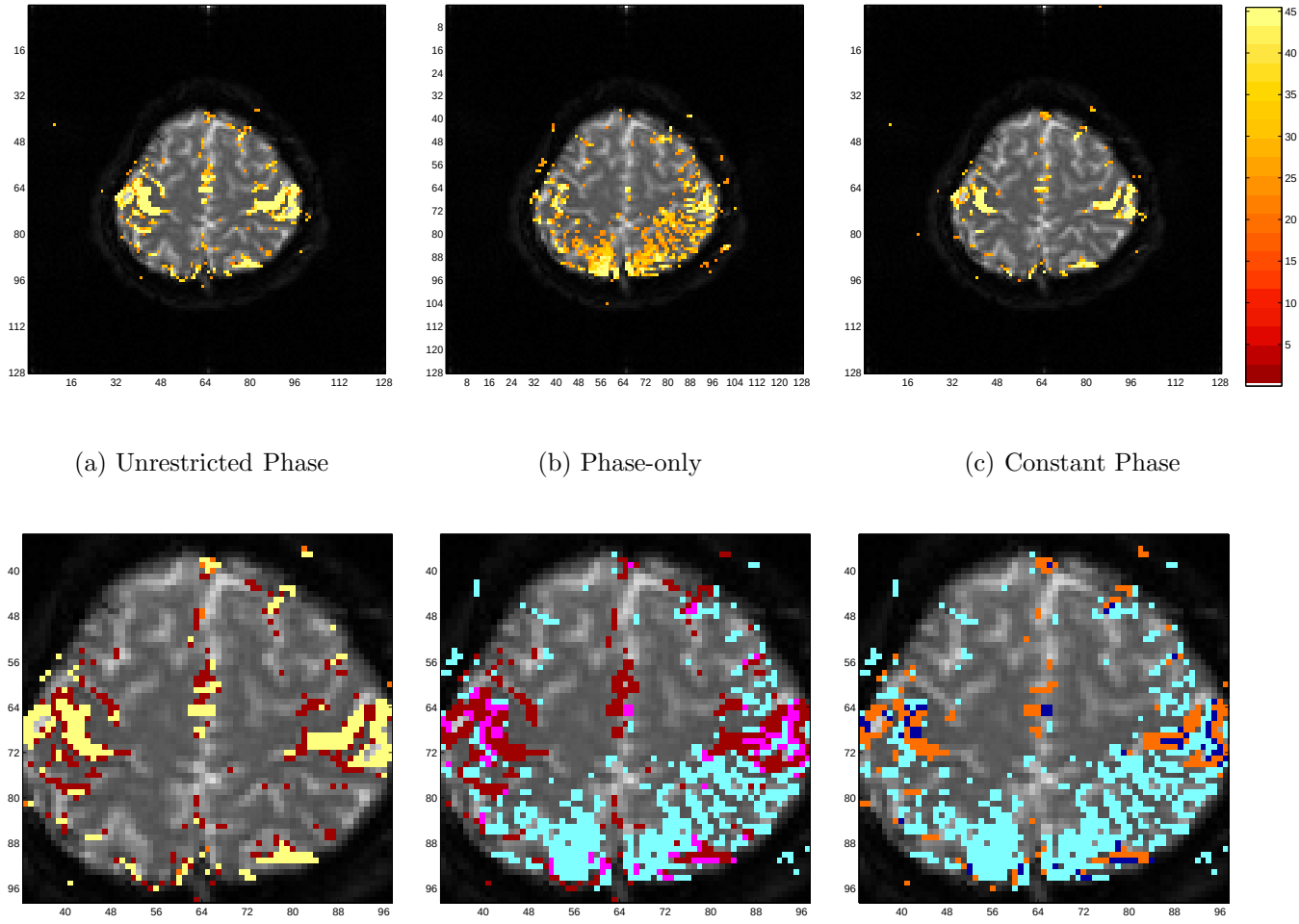

(a) Unrestricted Phase (b) Phase-only (c) Constant Phase

(d) Overlap map UP & CP (e) Overlap map UP & PO (f) Overlap map CP & PO

in to a central 64×64 section for (d) the models in (a) and (b); (e) the models in (a) and (c); and (f) the models in (b) and (c). Additionally, the same χ^2-statistic and overlap maps are presented in Fig. 4a-g except a 5% Bonferroni FWE thresholded is applied. In Fig. 3d-f and Fig. 4d-f, voxels that were above threshold for the UP model are colored red, for the CP model colored orange, for the UP & CP models colored yellow, for the PO model are colored light blue, for the UP & PO models colored pink, for the CP & PO models colored dark blue.

It can be seen from the FDR and FWE activation maps in Figs. 3 and 4 that the complex unrestricted phase model declares many voxels as active that have statistically

significant TRPC and that the Rowe-Logan complex activation model with a constant phase biases against voxels with TRPC as seen by fewer voxels colored dark blue than pink. This phenomenon is more prominent for a Bonferroni threshold.

For the same data, the χ^2 activation maps from the five hypothesis pairs from the current complex linear phase (LP) model are applied and presented in Fig. 5a-e with a colorbar to the right of Fig. 5c. Different hypothesis pairs of the current complex linear TRPC model are sensitive to different things. The properties of this model are pictorially presented in Figs. 5 and 6. It can be seen that the hypothesis test pair H_d vs H_c in Fig. 5c and the pair H_b vs H_a in Fig. 5e are very similar to the CP activation map. This similarity is because in the null hypotheses is no task related magnitude changes and in the alternative hypotheses are unrestricted task related magnitude changes. Further, the test pairs H_d vs H_b and H_c vs H_a are very similar to the UP activation map. This similarity is because in the null hypotheses is no task related phase changes and in the alternative hypotheses are unrestricted task related phase changes. In addition, the pair H_d vs H_a appears to be a combined UP & PO activation map because the null hypotheses is no task related magnitude and/or phase changes and in the alternative hypotheses are unrestricted task related magnitude and/or phase changes. In Fig. 5f is a two sided Bonferroni FWE corrected activation map for the PO model in which it can be noted that the activations in the sensorimotor area are positive (yellow) while others are negative (light blue) with a colorbar to the right. Perhaps one sided tests involving the phase are more appropriate.

In Fig. 6a-f are maps of overlapping voxels zoomed in for a central 64×64 portion that are above a 5% Bonferroni FWE threshold for the UP model, the PO model, and individually each of the maps given in Fig. 5a-e and Fig. 4a-c.

In Fig. 6 red indicates voxels that are above threshold only for the UP model; light blue indicates voxels that were above threshold only for the PO model; orange indicates voxels that are above threshold only for the appropriate complex model; light green indicates voxels that are above threshold voxels for all three models, the UP, PO, and the appropriate complex model; yellow indicates voxels that are above the threshold for both the UP and appropriate complex model; dark blue indicates voxels that are above threshold for both the PO and appropriate complex models; pink indicates voxels that are above the threshold for both the

Figure 5: Thresholded 5% FWE χ^2-statistic activation maps.

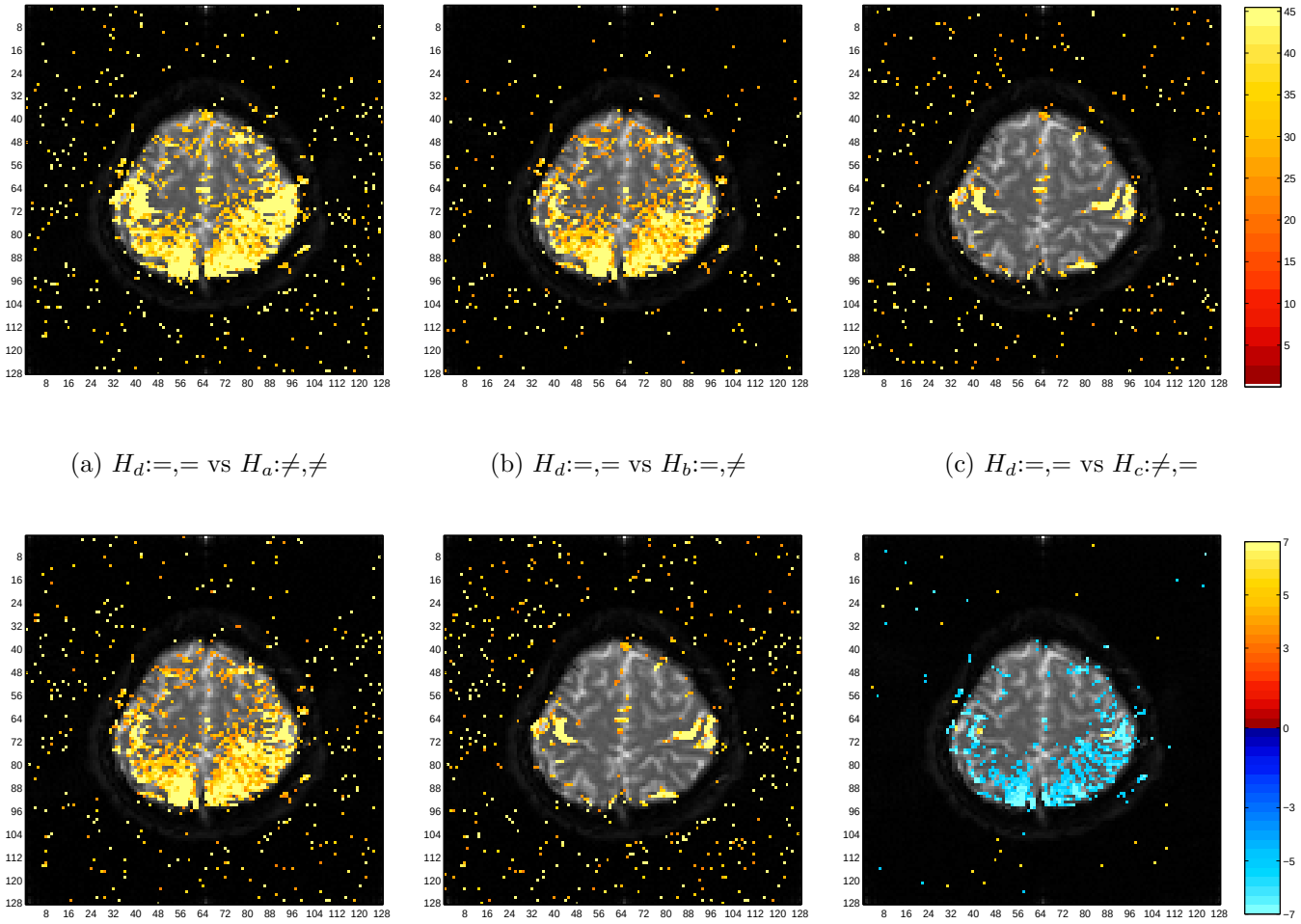

(a) H_d:=,= vs H_a:≠,≠ (b) H_d:=,= vs H_b:=,≠ (c) H_d:=,= vs H_c:≠,=

(d) H_c:≠,= vs H_a:≠,≠ (e) H_b:=,≠ vs H_a:≠,≠ (f) PO

UP and PO models; and voxels that were not above threshold for any of the three models retained their anatomical grey scale value.

It can be seen that the overlapping voxel maps from the UP model, the PO model, and LP hypothesis test pairs H_d vs H_c in Fig. 6c and H_b vs H_a in Fig. 6e are very similar to the UP, PO, and CP overlap map in Fig. 6; the overlapping voxel maps from the UP model, the PO model, and the LP hypothesis test pairs H_d vs H_b and H_c vs H_a are very similar to the PO activation map; while the UP model, the PO model, and pair H_d vs H_a appears to be a combined UP & PO overlap map.

Figure 6: Thresholded 5% FWE overlap maps.

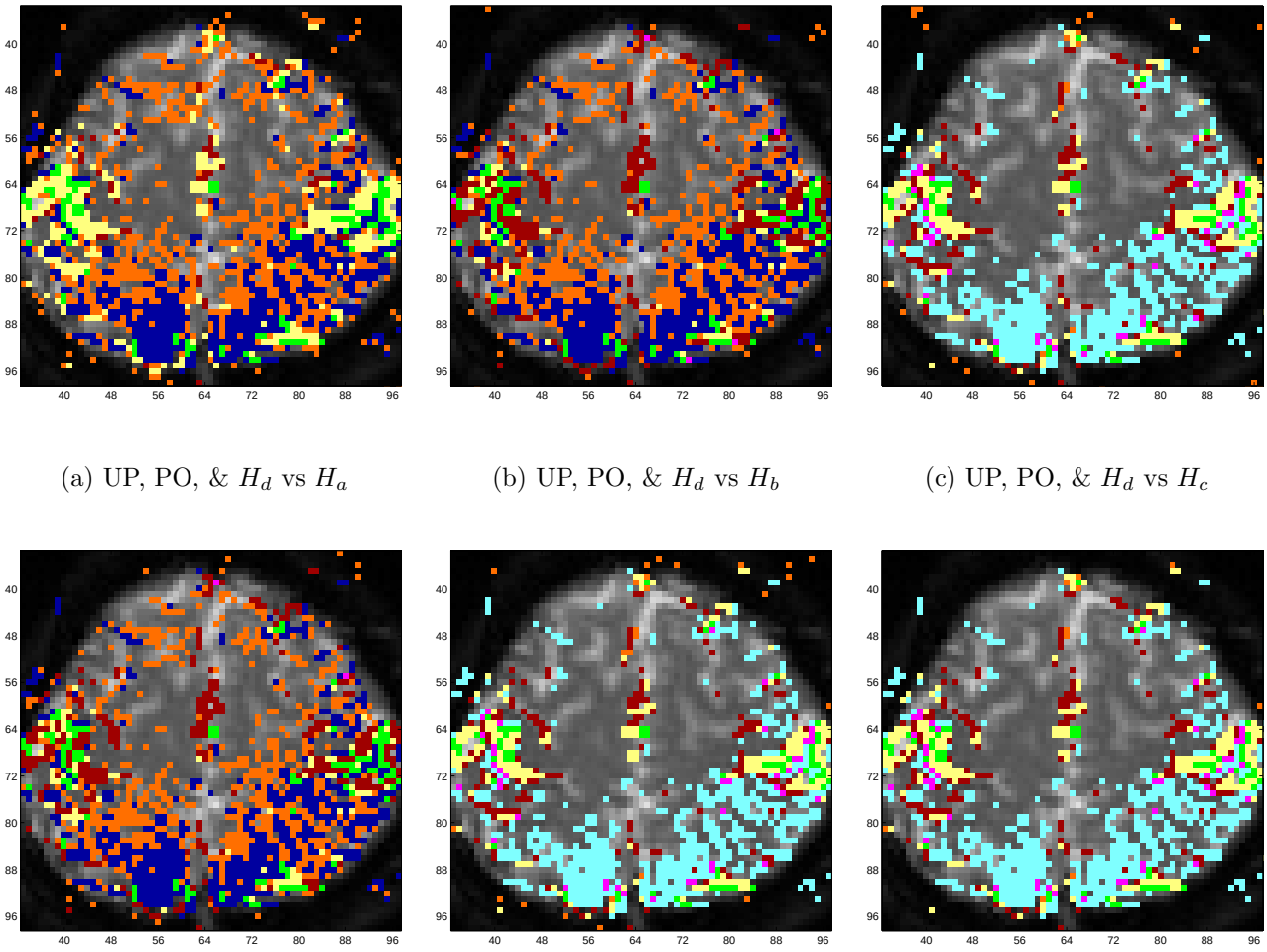

(a) UP, PO, & H_d vs H_a

(b) UP, PO, & H_d vs H_b

(c) UP, PO, & H_d vs H_c

(d) UP, PO, & H_c vs H_a

(e) UP, PO, & H_b vs H_a

(f) UP, PO, & CP

5 Simulated fMRI Data

Data are generated to simulate voxel activation from a block design fMRI experiment similar to that of Rowe and Logan (2004) except here, there are six areas of activation that are 5×5. The block design consisted of 16s off followed by eight epochs of 16s on and 16s off with an observation interval of one second or a TR= 1000ms. To mimic real data that requires magnetic field stabilization, the first three observations were omitted. The simulation consisted of $n = 269$ points where the true activation structure is known to be within the regions of interest (ROIs) so that the models can be evaluated.

Simulated fMRI data is constructed according to the previously described complex time course multiple regression model with a magnitude design matrix X and a phase design matrix U. The magnitude design matrix is specified to have three columns, the first a column of ones for intercept, the second a column of counting numbers (centered about the mean time) for a linear time trend, and the third a square wave reference function related to a block experimental design. For simplicity, the phase design matrix is taken to be the same as the magnitude design matrix. This model dictates that at time t,

$$\begin{aligned} y_t &= [(\beta_0 + \beta_1 t + \beta_2 x_{2t}) \cos(\gamma_0 + \gamma_1 t + \gamma_2 x_{2t}) + \eta_{Rt}] \\ &+ i[(\beta_0 + \beta_1 t + \beta_2 x_{2t}) \sin(\gamma_0 + \gamma_1 t + \gamma_2 x_{2t}) + \eta_{It}], \end{aligned} \tag{5.1}$$

where η_{Rt} and η_{It} are i.i.d. N(0,σ^2).

In this simulation study, the intercept and observation error standard deviation for all voxels was selected to be $\beta_1 = 0.00001$, and $\sigma = 0.04909$ which are values taken from a "highly active" voxel [16]. Therefore since the variance is held fixed, the SNR within a square 64×64 region similar to the the brain region in the real data is parameterized by varying β_0 so that the ratio SNR= β_0/σ takes on values 5.0 and 30, where 30 is approximately the value of SNR found in "highly active" voxels, and smaller values represent decreased SNR. The coefficient for the reference function β_2 within the ROIs has a value determined by a contrast-to-noise ratio (CNR=β_2/σ).

For the simulation, the phase was assigned to follow a linear model $\theta_t = \gamma_0 + \gamma_1 t + \gamma_2 x_{2t}$ or have a task related phase change (TRPC) γ_2. In all voxels $\gamma_0 = \pi/6$, $\gamma_1 = 0.00001$ and for all voxels outside the four ROIs $\gamma_2 = 0$. In the five ROIs lightened in Fig. 7, the (CNR,TRPC) values in order for numerically increasing ROIs $(1/4, 0)$, $(1/2, \pi/180)$, $(1/4, \pi/180)$, $(1/2, \pi/36)$, $(1/4, \pi/36)$, and $(0, \pi/180)$. The TRPC of $\pi/36$ is consistent with previous "large" vessel results [11]. Simulated data as just described are generated 1000 times.

In Fig. 8a-c are the 5% Bonferroni FWE detection power maps or percent of the time that the given voxel was above the threshold with simulated data at an SNR = 30 for the (a) complex UP (usual magnitude-only data) model, (b) PO model, (c) the Rowe-Logan complex CP activation model, (d)-(h) the current complex linear regression modeled TRPC activation under five different hypothesis pairs with simulated data at a SNR = 30. The same power maps are presented in Fig. 9 except with a SNR = 5.

Figure 7: Anatomical with ROIs.

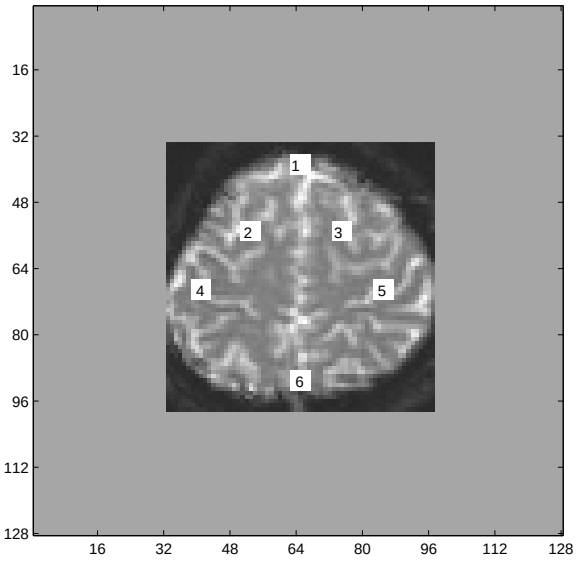

From Figs. 8 and 9 it can be seen that unrestricted phase (magnitude-only data) model detects task related changes in the magnitude regardless of whether or not there is TRPC but is decreased for decreased CNR and the phase-only data model detects task related changes in the phase regardless of whether or not there is task related magnitude changes but is decreased for the lower TRPC value for the lower SNR. The Rowe-Logan complex activation model with a constant phase exhibits the same power to detect task related magnitude changes when no TRPC is present. The complex constant phase model exhibits lower power when TRPC is present or biases against voxels with TRPC when the SNR is high. This appears to be the reason why in the real data there were voxels that were above the Bonferroni FWE threshold for the unrestricted phase model but not for the Rowe-Logan constant phase model because of its bias against voxels that demonstrate TRPC which are potentially ones with large vessels. It appears to focus on voxels with only task related changes in the magnitude and not those that also demonstrate TRPC unless the CNR is very high such as those in parenchymal tissue. The current complex linear TRPC model was implemented with five hypothesis pairs. The hypothesis pair H_d vs H_a detects task related activation either in the magnitude, the phase or both but has low power regardless of SNR for the low

Figure 8: χ^2-statistic 5% FWE detection power maps SNR=30.

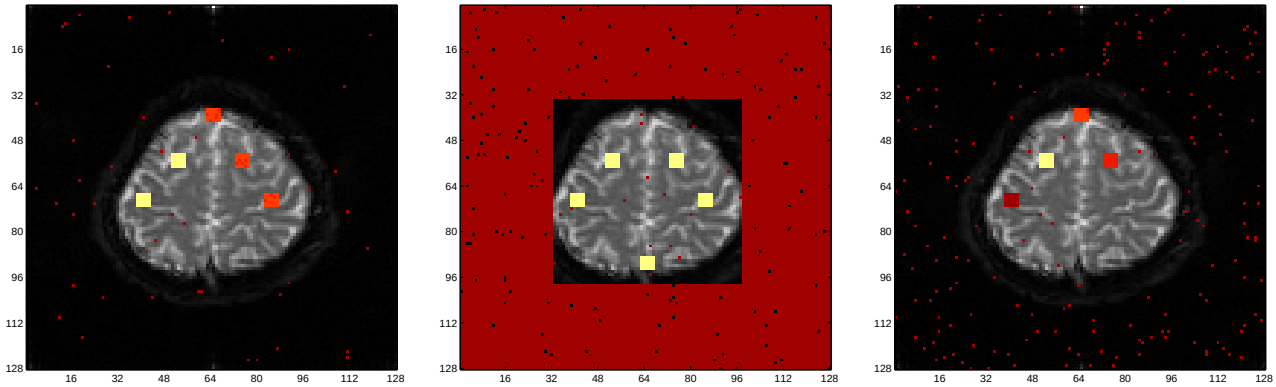

(a) Unrestricted Phase (b) Phase-Only Data (c) Constant Phase

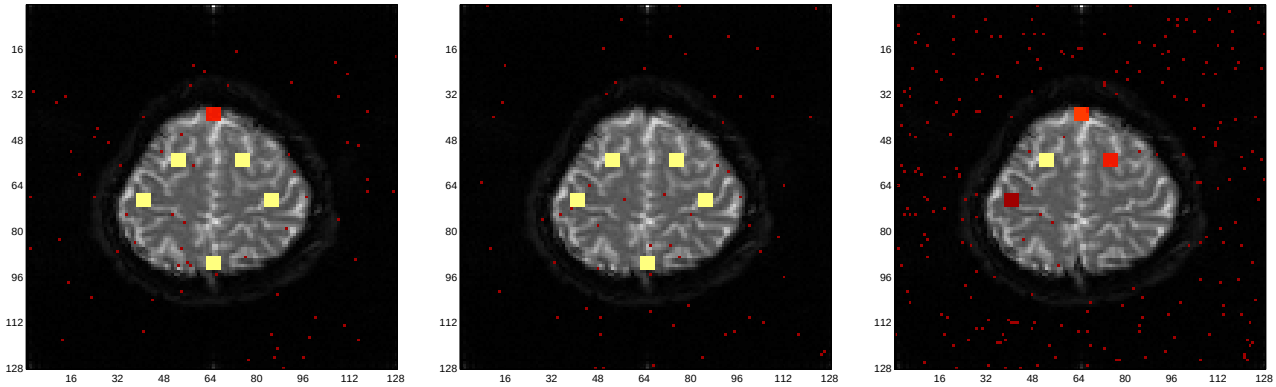

(d) H_d:=,= vs H_a:≠,≠ (e) H_d:=,= vs H_b:=,≠ (f) H_d:=,= vs H_c:≠,=

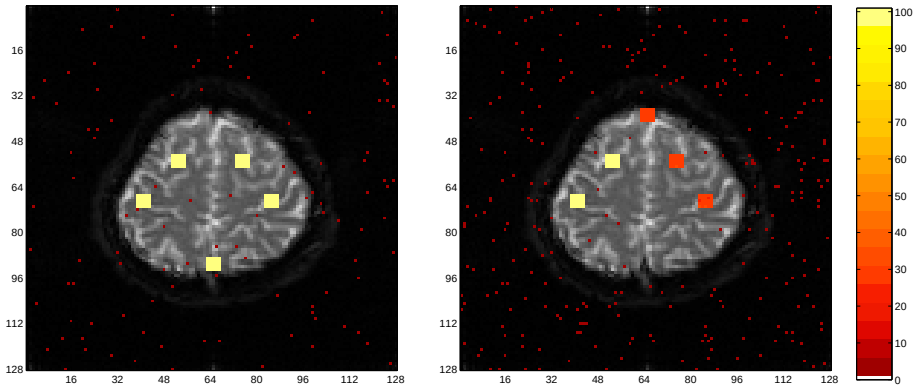

(g) H_c:≠,= vs H_a:≠,≠ (h) H_b:=,≠ vs H_a:≠,≠

Figure 9: χ^2-statistic 5% FWE detection power maps SNR=5.

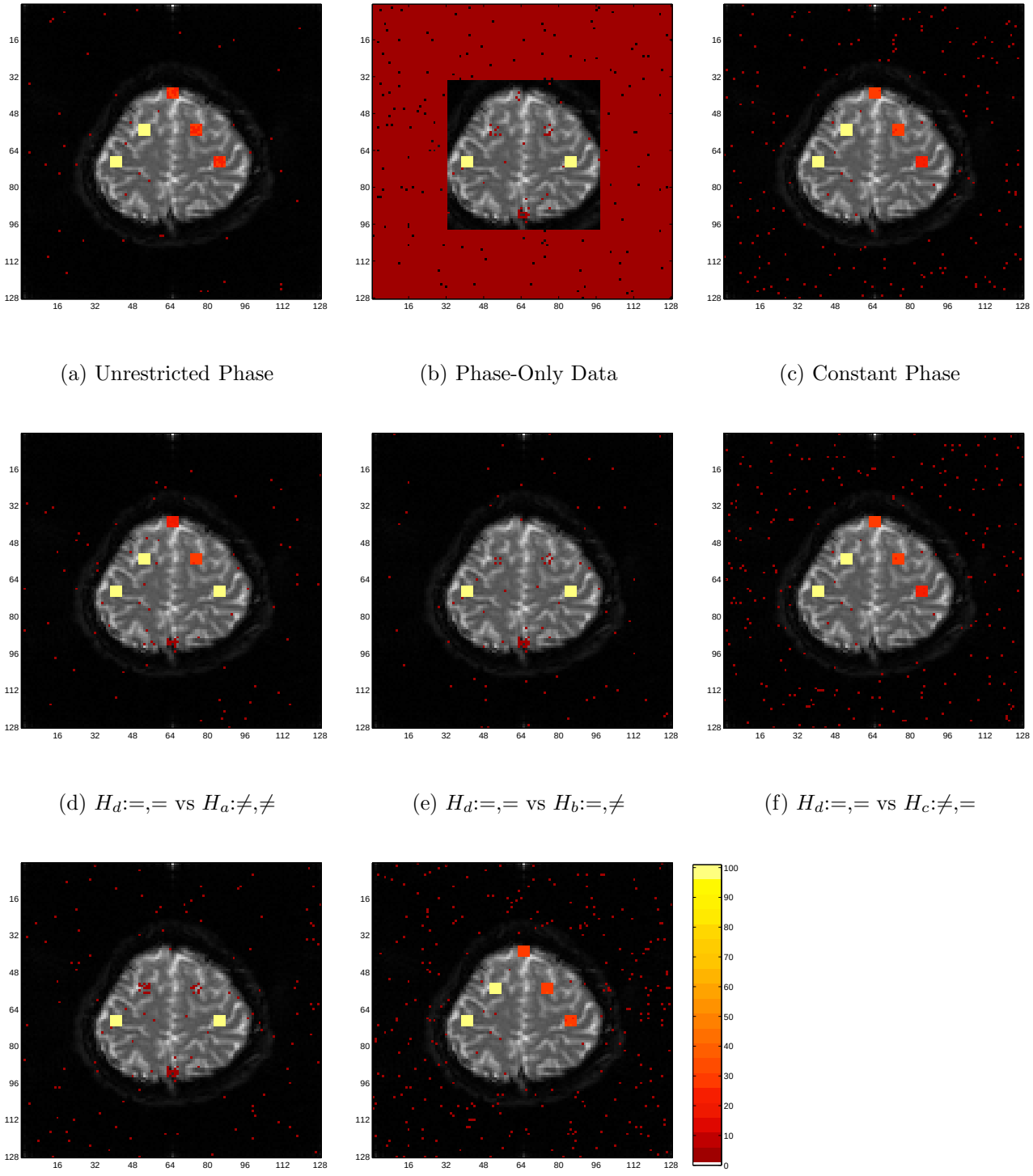

(a) Unrestricted Phase

(b) Phase-Only Data

(c) Constant Phase

(d) H_d:=,= vs H_a:≠,≠

(e) H_d:=,= vs H_b:=,≠

(f) H_d:=,= vs H_c:≠,=

(g) H_c:≠,= vs H_a:≠,≠

(h) H_b:=,≠ vs H_a:≠,≠

(CNR,TRPC) combination and low phase activation combination; H_d vs H_b detects task related activation in the phase regardless of whether or not there is task related changes in the magnitude but loses its ability to detect phase activation at the lower SNR; H_d vs H_c detects task related activation in the magnitude strongly biasing against voxels with TRPC when the SNR is high much like the constant phase model; H_c vs H_a detects task related activation in the phase regardless of whether or not there is task related changes in the magnitude but loses its ability to detect phase activation at the lower SNR; H_b vs H_a detects task related activation in the magnitude regardless of whether the phase has TRPC and regardless of SNR.

6 Conclusions

A generalization of the Rowe-Logan complex activation model was developed that specifically allows for modeling task related changes in both the magnitude and phase. Hypotheses regarding task related magnitude and phase changes are evaluated using derived activation statistics. Activation maps were generated on real data and activation power maps on simulated data for the unrestricted phase or magnitude-only data model, a phase-only data model, the Rowe-Logan constant phase model, and five hypothesis pairs of a newly introduced linear phase model. It was found that the magnitude-only data model declares voxels as active regardless of any phase changes, phase-only data model declares voxels as active regardless of any magnitude changes, and the five complex linear phase models were sensitive to different (CNR,TRPC) combinations. The current complex linear phase model is very general and includes all previously introduced activation models as special cases. Perhaps this model will reach its full potential with other experimental data acquisition methods such as flow tagging or steady state free precession.

A Generalized Likelihood Ratio Test

Upon converting from rectangular coordinates (y_{Rt}, y_{It}) in Eq. 2.1 to magnitude and phase polar coordinates (r_t, ϕ_t) the observed data at time point t can be represented as a 2×1 vector instead of as a complex number

$$\begin{pmatrix} r_t \cos\phi_t \\ r_t \sin\phi_t \end{pmatrix} = \begin{pmatrix} \rho_t \cos\theta_t \\ \rho_t \sin\theta_t \end{pmatrix} + \begin{pmatrix} \eta_{Rt} \\ \eta_{It} \end{pmatrix}, \qquad t = 1, \ldots, n$$

where r_t and ϕ_t are the observed magnitude and phase at time t.

With the aforementioned distributional specifications, the joint distribution of the complex or bivariate observation (y_{Rt}, y_{It}) at time t is

$$p(y_{Rt}, y_{It}|\rho_t, \theta_t, \sigma^2) = (2\pi\sigma^2)^{-\frac{2}{2}} \exp\left\{-\frac{(y_{Rt} - \rho_t\cos\theta_t)^2 + (y_{It} - \rho_t \sin\theta_t)^2}{2\sigma^2}\right\},$$

which upon making the transformation $(y_{Rt}, y_{It}) = (r_t\cos\phi_t, r_t\sin\phi_t)$ from rectangular coordinates to polar coordinates with Jacobian of the transformation $J(y_{Rt}, y_{It} \rightarrow r_t, \phi_t) = r_t$ and some algebra is

$$p(r_t, \phi_t|\rho_t, \theta_t, \sigma^2) = \frac{r_t}{2\pi\sigma^2} \exp\left\{-\frac{r_t^2 + \rho_t^2 - 2r_t\rho_t\cos(\phi_t - \theta_t)}{2\sigma^2}\right\}.$$

Under appropriate restricted hypotheses, the Lagrange constraints $\psi'(C\beta - 0)$ and $\delta'(D\gamma - 0)$ need to be added to the logarithm of the likelihood.

Maximizing this likelihood with respect to the parameters is the same as maximizing the logarithm of the likelihood LL with respect to the parameters. With n temporal observations the logarithm of the likelihood is

$$\begin{aligned} LL &= -n\log(2\pi) - \sum_{t=1}^{n}\log r_t - n\log\sigma^2 - \frac{1}{2\sigma^2}\sum_{t=1}^{n}\left[r_t^2 + (x_t'\beta)^2 - 2(x_t'\beta)r_t\cos(\phi_t - u_t'\gamma)\right] \\ &= -n\log(2\pi) - \sum_{t=1}^{n}\log r_t - n\log\sigma^2 - \frac{1}{2\sigma^2}\left[(r - X\beta)'(r - X\beta) + 2(r - r_*)'X\beta\right] \quad \text{(A.1)} \end{aligned}$$

where the linear representations of ρ_t and θ_t have been used while r has t^{th} element r_t and r_* has t^{th} element $r_t\cos(\phi_t - u_t'\gamma)$.

The likelihood ratio statistic is computed by maximizing the logarithm of the likelihood LL with respect to the parameters in β, γ, and σ^2 under the appropriate null and alternative

hypotheses. Denote the maximized values under the null hypothesis by $(\tilde{\beta}, \tilde{\gamma}, \tilde{\sigma}^2)$ and those under the alternative hypothesis as $(\hat{\beta}, \hat{\gamma}, \hat{\sigma}^2)$. These maximized values are then substituted into the likelihoods and the ratio taken.

Then the generalized likelihood ratio is

$$\lambda = \frac{p(r, \phi|\tilde{\beta}, \tilde{\gamma}, \tilde{\sigma}^2, X, U)}{p(r, \phi|\hat{\beta}, \hat{\gamma}, \hat{\sigma}^2, X, U)} = \frac{(\tilde{\sigma}^2)^{-2n/2} \exp\left\{-\left[(r - X\tilde{\beta})'(r - X\tilde{\beta}) + 2(r - \tilde{r}_*)'X\tilde{\beta}\right]/(2\tilde{\sigma}^2)\right\}}{(\hat{\sigma}^2)^{-2n/2} \exp\left\{-\left[(r - X\hat{\beta})'(r - X\hat{\beta}) + 2(r - \hat{r}_*)'X\hat{\beta}\right]/(2\hat{\sigma}^2)\right\}} \quad \text{(A.2)}$$

and Eq. 3.1 for the GLRT follows.

B Hypotheses

With this model, there are four linear hypotheses that can readily be seen and combined pairwise in several different ways to test distinct hypotheses. The parameters are estimated under each of the hypotheses so that pairs of hypotheses can be used in a generalized likelihood ratio test. Let C and D be $r_1 \times (q_1 + 1)$ and $r_2 \times (q_2 + 1)$ matrices of full row rank containing the linear hypothesis constraints in the following.

B.1 $H_a : C\beta \neq 0,\ D\gamma \neq 0$

For hypothesis a of unrestricted magnitude and phase, the logarithm of the likelihood is differentiated without any restrictions. Differentiation of the logarithm of the likelihood with respect to the magnitude regression coefficients β proceeds as follows

$$\begin{aligned} \frac{\partial LL}{\partial \beta} &= -\frac{1}{2\sigma^2}\frac{\partial}{\partial \beta}\left[(r - X\beta)'(r - X\beta) + 2(r - r_*)'X\beta\right] \\ &= -\frac{1}{2\sigma^2}\frac{\partial}{\partial \beta}\left[-2X'r - 2X'X\beta + 2X'(r - r_*)\right]. \end{aligned}$$

By setting this derivative equal to zero, annoting the parameters with hats, and solving, we get the MLE estimator under the unrestricted model given in Eq. B.3

Differentiation of the logarithm of the likelihood with respect to the phase regression

coefficients γ proceeds as follows

$$\begin{aligned}
\frac{\partial LL}{\partial \gamma} &= -\frac{1}{2\sigma^2}\frac{\partial}{\partial \gamma}\sum_{t=1}^{n}\left[r_t^2 + (x_t'\beta)^2 - 2(x_t'\beta)r_t\cos(\phi_t - u_t'\gamma)\right] \\
&\approx \frac{1}{\sigma^2}\frac{\partial}{\partial \gamma}\sum_{t=1}^{n} r_t(x_t'\beta)\left[1 - (\phi_t - u_t'\gamma)/2\right] \\
&= \frac{1}{\sigma^2}\frac{\partial}{\partial \gamma}\sum_{t=1}^{n}\left[r_t(x_t'\beta) - (\phi_{t*} - z_t'\gamma)/2\right] \\
&= \frac{1}{\sigma^2}\frac{\partial}{\partial \gamma}\left[r'X\beta - \frac{1}{2}(\phi_* - Z\gamma)'(\phi_* - Z\gamma)\right] \\
&= \frac{1}{\sigma^2}\left[-2Z'\phi_* + 2Z'Z\gamma\right]
\end{aligned}$$

where $\hat{\phi}_*$ is an $n \times 1$ vector with t^{th} element $\phi_{t*} = \phi_t\sqrt{r_t x_t'\beta}$, and Z is an $n \times (q_2 + 1)$ matrix with t^{th} row $z_t' = u_t'\sqrt{r_t(x_t'\beta)}$. By setting this derivative equal to zero, annoting the parameters with hats, and solving, we get the MLE estimator in Eq. B.3. Note that a Taylor series approximation to the cosine was used. This approximation is robust to a mild difference in its argument $\alpha = \phi_t - u_t'\gamma$. For example, if $\alpha = \pi/12$ radians or 15 degrees, the exact cosine is 0.9659 while the approximation yields 0.9657. Results from previous literature [11] find that the phase may deviate from its mean by as much as 5 degrees in voxels with large vessels. Note that the same result is found by differentiating the cosine exactly and approximating the resulting sinusoid,

$$\begin{aligned}
\frac{\partial}{\partial \gamma}\cos(\phi_t - u_t'\gamma) &= -u_t\sin(\phi_t - u_t'\gamma) \\
&\approx -u_t(\phi_t - u_t'\gamma)\ .
\end{aligned}$$

Differentiation of the logarithm of the likelihood with respect to the variance σ^2 proceeds as follows

$$\frac{\partial LL}{\partial \sigma^2} = -n\left(\sigma^2\right)^{-1} - \frac{1}{2}\left[(r - X\beta)'(r - X\beta) + 2(r - r_*)'X\beta\right](\sigma^2)^{-2}\ .$$

By setting this derivative equal to zero, annoting the parameters with hats, and solving, we get the MLE under the unrestricted model given in Eq. B.3.

The maximum likelihood estimators under this hypothesis are given by

$$\begin{aligned}
\hat{\beta} &= (X'X)^{-1}X'\hat{r}_*, \\
\hat{\gamma} &= (\hat{Z}'\hat{Z})^{-1}\hat{Z}'\hat{\phi}_*, \\
\hat{\sigma}^2 &= \frac{1}{2n}\left[(r - X\hat{\beta})'(r - X\hat{\beta}) + 2(r - \hat{r}_*)'X\hat{\beta}\right] ,
\end{aligned} \tag{B.3}$$

where $\hat{r}_*$ is an $n \times 1$ vector with t^{th} element $r_t \cos(\phi_t - u_t'\hat{\gamma})$, $\hat{Z}$ is an $n \times (q_2 + 1)$ matrix with t^{th} row $\hat{z}_t' = u_t'\sqrt{r_t x_t'\hat{\beta}}$, $\hat{\phi}_*$ is an $n \times 1$ vector with t^{th} element $\phi_t\sqrt{r_t x_t'\hat{\beta}}$, and r is an $n \times 1$ vector of observed magnitudes. In deriving the MLE $\hat{\gamma}$, an approximation was made for a cosine term.

B.2 $H_b : C\beta = 0,\ D\gamma \neq 0$

For hypothesis b of restricted magnitude but not phase, the logarithm of the likelihood is differentiated with the added Lagrange restriction $\psi'(C\beta - 0)$. Differentiation of the logarithm of the likelihood that includes the Lagrange constraint with respect to the magnitude regression coefficients β proceeds as follows

$$\begin{aligned}
\frac{\partial LL}{\partial \beta} &= \frac{\partial}{\partial \beta}\left\{\frac{1}{2\sigma^2}\left[(r - X\beta)'(r - X\beta) + 2(r - r_*)'X\beta\right] + \psi'(C\beta - 0)\right\} \\
&= -\frac{1}{2\sigma^2}\left[-2X'r - 2X'X\beta + 2X'(r - r_*)\right] + C'\psi
\end{aligned}$$

where the variables are as previously defined. By setting this derivative equal to zero, annoting the parameters with breves, and solving, we get the MLE estimator in Eq. B.4 below.

Differentiation of the logarithm of the likelihood with respect to the phase regression

coefficients γ proceeds as follows

$$\begin{aligned}
\frac{\partial LL}{\partial \gamma} &= -\frac{\partial}{\partial \gamma}\left\{\frac{1}{2\sigma^2}\sum_{t=1}^{n}\left[r_t^2 + (x_t'\beta)^2 - 2(x_t'\beta)r_t\cos(\phi_t - u_t'\gamma)\right]\right\} \\
&\approx \frac{\partial}{\partial \gamma}\left\{\frac{1}{2\sigma^2}\sum_{t=1}^{n} r_t(x_t'\beta)\left[1 - (\phi_t - u_t'\gamma)/2\right]\right\} \\
&= \frac{\partial}{\partial \gamma}\left\{\frac{1}{2\sigma^2}\sum_{t=1}^{n}\left[r_t(x_t'\beta) - (\phi_{t*} - z_t'\gamma)/2\right]\right\} \\
&= \frac{\partial}{\partial \gamma}\left\{\frac{1}{2\sigma^2}\left[r'X\beta - \frac{1}{2}(\phi_* - Z\gamma)'(\phi_* - Z\gamma)\right]\right\} \\
&= \frac{1}{2\sigma^2}\left[-2Z'\phi_* + 2Z'Z\gamma\right]
\end{aligned}$$

where the variables are as previously defined. By setting this derivative equal to zero, annoting the parameters with breves, and solving, we get the MLE estimator in Eq. B.4 below.

Differentiation of the logarithm of the likelihood with respect to the variance σ^2 proceeds as follows

$$\frac{\partial LL}{\partial \sigma^2} = -n\left(\sigma^2\right)^{-1} - \frac{1}{2}\left[(r - X\beta)'(r - X\beta) + 2(r - r_*)'X\beta\right](\sigma^2)^{-2} .$$

By setting this derivative equal to zero, annoting the parameters with breves, and solving, we get the MLE under the unrestricted model given in Eq. B.4 below.

The maximum likelihood estimators under this hypothesis are given by

$$\begin{aligned}
\breve{\beta} &= \Psi(X'X)^{-1}X'\breve{r}_*, \\
\breve{\gamma} &= (\breve{Z}'\breve{Z})^{-1}\tilde{Z}'\breve{\phi}_*, \\
\breve{\sigma}^2 &= \frac{1}{2n}\left[(r - X\breve{\beta})'(r - X\breve{\beta}) + 2(r - \breve{r}_*)'X\breve{\beta}\right] , \\
\Psi &= I_{q_1+1} - (X'X)^{-1}C'[C(X'X)^{-1}C']^{-1}C/,
\end{aligned}$$

where $\breve{r}_*$ is an $n \times 1$ vector with t^{th} element $\breve{r}_t\cos(\phi_t - u_t'\breve{\gamma})$, $\breve{Z}$ is an $n \times (q_2 + 1)$ matrix with t^{th} row $\breve{z}_t' = u_t'\sqrt{r_t x_t'\breve{\beta}}$, $\breve{\phi}_*$ is an $n \times 1$ vector with t^{th} element $\phi_t\sqrt{r_t x_t'\breve{\beta}}$, and r is as above. In computing maximum likelihood estimates, an iterative maximization algorithm [8, 14, 15] is used.

B.3 $H_c : C\beta \neq 0,\ D\gamma = 0$

For hypothesis c of restricted phase but not magnitude, the logarithm of the likelihood is differentiated with the added Lagrange restrictions $\delta'(D\gamma - 0)$. Differentiation of the logarithm of the likelihood that includes the Lagrange constraints with respect to the phase regression coefficients β proceeds as follows

$$\begin{aligned}\frac{\partial LL}{\partial \beta} &= \frac{\partial}{\partial \beta}\left\{\frac{1}{2\sigma^2}\left[(r - X\beta)'(r - X\beta) + 2(r - r_*)'X\beta\right] + \delta'(D\gamma - 0)\right\} \\ &= -\frac{1}{2\sigma^2}\left[-2X'r - 2X'X\beta + 2X'(r - r_*)\right]\end{aligned}$$

where the variables are as previously defined. By setting this derivative equal to zero, annoting the parameters with bars, and solving, we get the MLE estimator in Eq. B.4 below.

Differentiation of the logarithm of the likelihood that includes the Lagrange constraints with respect to the phase regression coefficients γ proceeds as follows

$$\begin{aligned}\frac{\partial LL}{\partial \gamma} &= -\frac{\partial}{\partial \gamma}\left\{\frac{1}{2\sigma^2}\sum_{t=1}^{n}\left[r_t^2 + (x_t'\beta)^2 - 2(x_t'\beta)r_t\cos(\phi_t - u_t'\gamma)\right] + \delta'(D\gamma - 0)\right\} \\ &\approx \frac{\partial}{\partial \gamma}\left\{\frac{1}{2\sigma^2}\sum_{t=1}^{n} r_t(x_t'\beta)\left[1 - (\phi_t - u_t'\gamma)/2\right] + \delta' D\gamma\right\} \\ &= \frac{\partial}{\partial \gamma}\left\{\frac{1}{2\sigma^2}\sum_{t=1}^{n}\left[r_t(x_t'\beta) - (\phi_{t*} - z_t'\gamma)/2\right] + \delta' D\gamma\right\} \\ &= \frac{\partial}{\partial \gamma}\left\{\frac{1}{2\sigma^2}\left[r'X\beta - \frac{1}{2}(\phi_* - Z\gamma)'(\phi_* - Z\gamma)\right] + \delta' D\gamma\right\} \\ &= \frac{1}{2\sigma^2}\left[-2Z'\phi_* + 2Z'Z\gamma\right] + D'\delta\end{aligned}$$

where the variables are as previously defined. By setting this derivative equal to zero, annoting the parameters with bars, and solving, we get the MLE estimator in Eq. B.4 below.

Differentiation of the logarithm of the likelihood with respect to the variance σ^2 proceeds as follows

$$\frac{\partial LL}{\partial \sigma^2} = -n\left(\sigma^2\right)^{-1} - \frac{1}{2}\left[(r - X\beta)'(r - X\beta) + 2(r - r_*)'X\beta\right]\left(\sigma^2\right)^{-2}.$$

By setting this derivative equal to zero, annoting the parameters with bars, and solving, we get the MLE under the unrestricted model given in Eq. B.4 below.

The maximum likelihood estimators under this hypothesis are given by

$$\begin{aligned}
\bar{\beta} &= (X'X)^{-1}X'\bar{r}_*, \\
\bar{\gamma} &= \Omega(\tilde{Z}'\tilde{Z})^{-1}\bar{Z}'\bar{\phi}_*, \\
\bar{\sigma}^2 &= \frac{1}{2n}\left[(r - X\bar{\beta})'(r - X\bar{\beta}) + 2(r - \bar{r}_*)'X\bar{\beta}\right] , \\
\Omega &= I_{q_2+1} - (\bar{Z}'\bar{Z})^{-1}D'[D(\bar{Z}'\bar{Z})^{-1}D']^{-1}D
\end{aligned} \tag{B.4}$$

where $\bar{r}_*$ is an $n \times 1$ vector with t^{th} element $\bar{r}_t \cos(\phi_t - u_t'\bar{\gamma})$, $\bar{Z}$ is an $n \times (q_2 + 1)$ matrix with t^{th} row $\bar{z}_t' = u_t'\sqrt{r_t x_t'\tilde{\beta}}$, $\bar{\phi}_*$ is an $n \times 1$ vector with t^{th} element $\phi_t\sqrt{r_t x_t'\bar{\beta}}$, and r is as above. In computing maximum likelihood estimates, an iterative maximization algorithm is used [8, 14, 15].

B.4 $H_d : C\beta = 0,\ D\gamma = 0$

For hypothesis d of linearly restricted magnitude and phase, the logarithm of the likelihood is differentiated with the added Lagrange restrictions $\psi'(C\beta - 0)$ and $\delta'(D\gamma - 0)$. Differentiation of the logarithm of the likelihood that includes the Lagrange constraints with respect to the magnitude regression coefficients β proceeds as follows

$$\begin{aligned}
\frac{\partial LL}{\partial \beta} &= \frac{\partial}{\partial \beta}\left\{\frac{1}{2\sigma^2}\left[(r - X\beta)'(r - X\beta) + 2(r - r_*)'X\beta\right] + \psi'(C\beta - 0) + \delta'(D\gamma - 0)\right\} \\
&= -\frac{1}{2\sigma^2}\left[-2X'r - 2X'X\beta + 2X'(r - r_*)\right] + C'\psi
\end{aligned}$$

where the variables are as previously defined. By setting this derivative equal to zero, annoting the parameters with tildes, and solving, we get the MLE estimator in Eq. B.5.

Differentiation of the logarithm of the likelihood that includes the Lagrange constraints

with respect to the phase regression coefficients γ proceeds as follows

$$\begin{aligned}
\frac{\partial LL}{\partial \gamma} &= -\frac{\partial}{\partial \gamma}\left\{\frac{1}{2\sigma^2}\sum_{t=1}^{n}\left[r_t^2 + (x_t'\beta)^2 - 2(x_t'\beta)r_t\cos(\phi_t - u_t'\gamma)\right] + \psi'(C\beta - 0) + \delta'(D\gamma - 0)\right\} \\
&\approx \frac{\partial}{\partial \gamma}\left\{\frac{1}{2\sigma^2}\sum_{t=1}^{n} r_t(x_t'\beta)\left[1 - (\phi_t - u_t'\gamma)/2\right] + \delta' D\gamma\right\} \\
&= \frac{\partial}{\partial \gamma}\left\{\frac{1}{2\sigma^2}\sum_{t=1}^{n}\left[r_t(x_t'\beta) - (\phi_{t*} - z_t'\gamma)/2\right] + \delta' D\gamma\right\} \\
&= \frac{\partial}{\partial \gamma}\left\{\frac{1}{2\sigma^2}\left[r'X\beta - \frac{1}{2}(\phi_* - Z\gamma)'(\phi_* - Z\gamma)\right] + \delta' D\gamma\right\} \\
&= \frac{1}{2\sigma^2}\left[-2Z'\phi_* + 2Z'Z\gamma\right] + D'\delta
\end{aligned}$$

where the variables are as previously defined. By setting this derivative equal to zero, annoting the parameters with tildes, and solving, we get the MLE estimator in Eq. B.5.

Differentiation of the logarithm of the likelihood with respect to the variance σ^2 proceeds as follows

$$\frac{\partial LL}{\partial \sigma^2} = -n\left(\sigma^2\right)^{-1} - \frac{1}{2}\left[(r - X\beta)'(r - X\beta) + 2(r - r_*)'X\beta\right](\sigma^2)^{-2} \ .$$

By setting this derivative equal to zero, annoting the parameters with tildes, and solving, we get the MLE's under the unrestricted model given in Eq. B.5 below

The maximum likelihood estimators under this hypothesis are given by

$$\begin{aligned}
\tilde{\beta} &= \Psi(X'X)^{-1}X'\tilde{r}_*, \\
\tilde{\gamma} &= \Omega(\tilde{Z}'\tilde{Z})^{-1}\tilde{Z}'\tilde{\phi}_*, \\
\tilde{\sigma}^2 &= \frac{1}{2n}\left[(r - X\tilde{\beta})'(r - X\tilde{\beta}) + 2(r - \tilde{r}_*)'X\tilde{\beta}\right] \ , \\
\Psi &= I_{q_1+1} - (X'X)^{-1}C'[C(X'X)^{-1}C']^{-1}C \\
\Omega &= I_{q_2+1} - (\tilde{Z}'\tilde{Z})^{-1}D'[D(\tilde{Z}'\tilde{Z})^{-1}D']^{-1}D
\end{aligned} \tag{B.5}$$

where $\tilde{r}_*$ is an $n \times 1$ vector with t^{th} element $\tilde{r}_t\cos(\phi_t - u_t'\tilde{\gamma})$, $\tilde{Z}$ is an $n \times (q_2 + 1)$ matrix with t^{th} row $\tilde{z}_t' = u_t'\sqrt{r_t x_t'\tilde{\beta}}$, $\tilde{\phi}_*$ is an $n \times 1$ vector with t^{th} element $\phi_t\sqrt{r_t x_t'\tilde{\beta}}$, and r is as above. In computing maximum likelihood estimates under both hypotheses, an iterative maximization algorithm is used [8, 14, 15].

References

[1] P. Bandettini, A. Jesmanowicz, E. Wong, and J.S. Hyde. Processing strategies for time-course data sets in functional MRI of the human brain. *Magn. Reson. Med.*, 30(2):161–173, 1993.

[2] M.A. Bernstein, D.M. Thomasson, and W.H. Perman. Improved detectability in low signal-to-noise ratio magnetic resonance images by means of a phase-corrected real reconstruction. *Med. Phys.*, 16(5):813–817, 1989.

[3] R.W. Cox, A. Jesmanowicz, and J.S. Hyde. Real-time functional magnetic resonance imaging. *Magn. Reson. Med.*, 33(2):230–236, 1995.

[4] R.C. Gonzales and R.E. Woods. *Digital Image Processing*. Addison-Wesley Publishing Company, Reading, Massachusetts, 1992.

[5] H. Gudbjartsson and S. Patz. The Rician distribution of noisy data. *Magn. Reson. Med.*, 34(6):910–914, 1995.

[6] E.M. Haacke, R. Brown, M. Thompson, and R. Venkatesan. *Magnetic Resonance Imaging: Principles and Sequence Design*. John Wiley and Sons, New York, NY, USA, 1999.

[7] F.G. Hoogenrad, J.R. Reichenbach, E.M. Haacke, S. Lai, K. Kuppusamy, and M. Sprenger. In vivo measurement of changes in venous blood-oxygenation with high resolution functional MRI at .95 Tesla by measuring changes in susceptibility and velocity. *Magn. Reson. Med.*, 39(1):97–107, 1998.

[8] D.V. Lindley and A.F.M. Smith. Bayes estimates for the linear model. *J. R. Stat. Soc., B*, 34(1), 1972.

[9] B.R. Logan and D.B. Rowe. An evaluation of thresholding techniques in fMRI analysis. *NeuroImage*, 22(1):95–108, 2004.

[10] A. Macovski. Noise in MRI. *Magn. Reson. Med.*, 36(3):494–497, 1996.

[11] R.S. Menon. Postacquisition suppression of large-vessel BOLD signals in high-resolution fMRI. *Magn. Reson. Med.*, 47(1):1–9, 2002.

[12] W.H. Press, S.A. Teukolsky, W.T. Vetterling, and B.P. Flannery. *Numerical Recipies in C*. Cambridge University Press, Cambridge, UK, second edition, 1992.

[13] S.O. Rice. Mathematical analysis of random noise. *Bell system Tech. J.*, 23:282, 1944. Reprinted by N. Wax, Selected papers on Noise and Stochastic Process, Dover Publication, 1954. QA273W3.

[14] D.B. Rowe. Bayesian source separation for reference function determination in fMRI. *Magn. Reson. Med.*, 45(5):374–378, 2001.

[15] D.B. Rowe. *Multivariate Bayesian Statistics*. Chapman & Hall/CRC Press, Boca Raton, FL, USA, 2003.

[16] D.B. Rowe and B.R. Logan. A complex way to compute fMRI activation. *NeuroImage*, 23(3):1078–1092, 2004.

[17] D.B. Rowe and B.R. Logan. Complex fMRI analysis with unrestricted phase is equivalent to a magnitude-only model. *NeuroImage*, 24(1), 2005.